Mechanical Characterization of Foils with Compression in Their Planes

GIUSEPPE COCCHETTI[1], MOHAMMAD REZA MAHINI[2], and GIULIO MAIER[1]

[1]*Department of Structural Engineering, Politecnico di Milano, Milano, Italy*
[2]*Tarbiat Modares University, Tehran, Iran*

Received 5 April 2012; accepted 2 August 2012.

1. Introduction

At present, laminates consisting of several layers of diverse materials (usually paper, aluminum, and polymers) are employed for the production of food containers (billions per day around the world) and of other kinds of multiple products. Industrial processes and service conditions are often investigated to design purposes by advanced experimental and computational tools. Like in other modern engineering technologies, accurate simulations of complex mechanical behaviors require not only sophisticated "direct" structural analyses, emerged from past decades of developments in computers and computational procedures, but also realistic inputs are required for such procedures, namely, realistic models of material behaviors and accurate quantification of their parameters (see e.g., [1–4]). Such requirements can now be satisfied by inverse analysis, i.e., by a relatively recent and still growing methodology apt to perform the transition from effects to causes through simulations of suitably designed experiments. This is the approach and the kind of procedure investigated herein in view of the following circumstances.

Paperboards or laminates in walls of containers, in their corners as boxes, and in their folds of top and bottom closures, are subjected also to compression in service (not only to tension, bending, and shear). The laminate behavior in the presence of compression, if compared to that (by far more frequent) under dominant tension, exhibits two features: (i) there may be remarkable differences in the nonlinear inelastic range, and (ii) it is obviously difficult to test with compression in view of specimen instability and wrinkling. This article is intended as a contribution to solve the above practical problem.

The purpose pursued here is the design of a testing procedure with compression in the foil plane for the calibration of constitutive models in generalized variables (particularly axial force and bending moment) to be employed for simulations of mechanical responses to loadings of industrial products, specifically food containers, interpretable as assemblages of shells or plates as their walls.

In the present study, the foil sample is assumed to be homogeneous and it is finite element modeled as a continuum like the surrounding stabilizing "blocks" (also in view of some limitations of the adopted commercial code). After the calibration of the material model, the transition is carried out to a generalized variables model by means of a second, much simpler, identification of parameters.

This study is oriented to the industrial design and production and is intended to preliminarily propose various novelties of practical interest with respect to the state-of-the-art in pertinent engineering environments.

Address correspondence to Giulio Maier, Department of Structural Engineering, Politecnico di Milano, I-20133 Milano, Italy. E-mail: giulio.maier@polimi.it

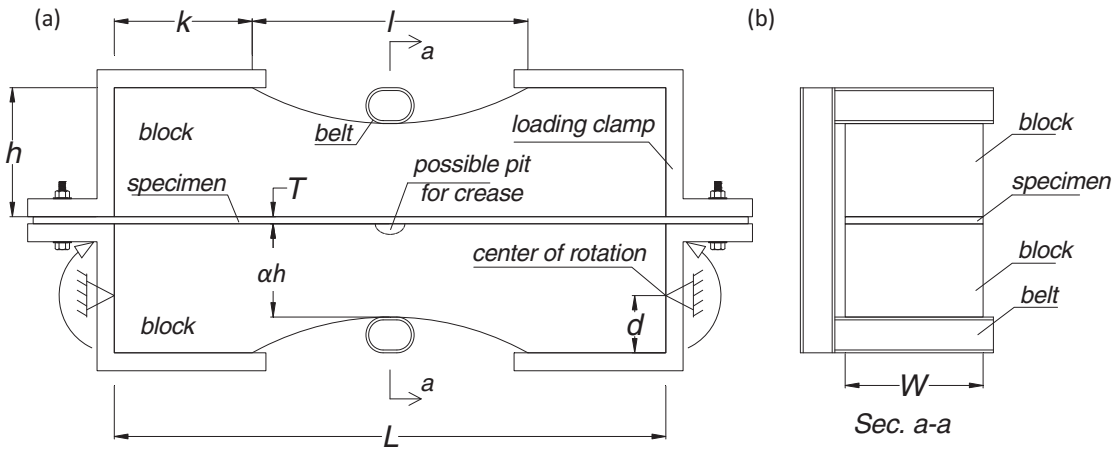

Fig. 1. Schematic representation of the "sandwich system." (a) Front view with the surface on which "full-field" displacements are measured by DIC. (b) Cross section a-a in the transversal plane of symmetry.

2. Preliminary Design

2.1. *The "Sandwich" Concept*

The general configuration of the "sandwich system" is visualized in Figure 1. A rectangular specimen of the foil is inserted between two stabilizing components called "stabilizers" or "blocks." The remarks that follow motivate the various features chosen in the design of this novel experimental equipment and its "modus operandi" proposed herein.

(a) The "blocks" are to be designed in order to fulfill the following requirements during each test: reversible ("holonomic") elastic behavior; realistic constitutive model with parameters accurately known once-for-all "a priori"; stability and no bifurcations in test responses of the specimen; for each category of foils (e.g., laminates, corrugated paperboard, or a set of single layers) two or more kinds of block pairs should be designed and made available in the laboratory for sandwich tests.

It is worth underlining that such blocks are rather economical: inexpensive material, such as polymers or rubber, with shapes easy to produce. Their shapes and dimensions (shown in Figure 1) must be consistent with those of the specimen, namely, length (L), width (W), and thickness (T) typical for each kind of samples. Stabilization of the specimen can be achieved, with modest operative complication, also by transversal "belts." As shown in Figure 1, here the belt consists of two transversal parallel horizontal bars with a stiff vertical connection on the back side of the sandwich in order to allow DIC measurements over the front side.

(b) The external actions on the above "sandwich system" (specimen + blocks) are imposed by two rigid metallic clamps rotating around axes located at an equal preselected level. Symmetry of the system with respect to the vertical central plane is preserved in the test, as indicated in Figure 1. The external frame supporting the sandwich clamps and the simple mechanism providing the external actions are not specified herein. Diverse operative actions are foreseen for sandwich testing: the two rotation hinges can be activated at the bottom basis of the clamps and of the frame in order to generate dominant compression in the foil sample; dominant flexure is generated in it if the hinges are placed near to the specimen level; intermediate placements can be adopted in order to achieve in the test a chosen balanced combination of compression and bending. The loading moments consequent to the imposed rotations of the clamps may represent experimental data measured at preselected stages of the test or recorded along the test as a function of the clamp rotation. Such data, if available, are additional to the essential numerous measurements of displacements provided by digital image correlation (DIC), as specified in Subsection 2.2. The surrounding equipment apt to accurately impose designed rotations or loads on the clamps is not investigated herein.

(c) As for the external actions, the following two alternatives are considered: (A) at preselected stages, which become measurement steps, two symmetrical rotations are imposed on the clamps and define the boundary conditions for the computer simulation of each step; (B) a force is applied by small jacks on each clamp so that the moment with respect to the hinge can be achieved as an additional kind of experimental data.

The above alternatives will be computationally compared in Subsection 5.2. Clearly, an increase of experimental data may improve the parameter identification procedure. However, with (B) the surrounding equipment (not investigated herein) in order to accurately impose designed rotations on the clamps would become more complex and costly if made apt to provide accurate measurements of corresponding loads. Moreover, with (B) softening overall behavior of the sandwich might imply instability. In the present context, in view of "a priori" simulations of the test at preselected measurement stages, these stages have to be pre-defined in terms of clamp rotations values. This is quite possible since the DIC equipment may provide a dense sequence of photographs (a sort of movie) among which the ones at preselected clamps rotations can be exploited for the inverse analysis procedure.

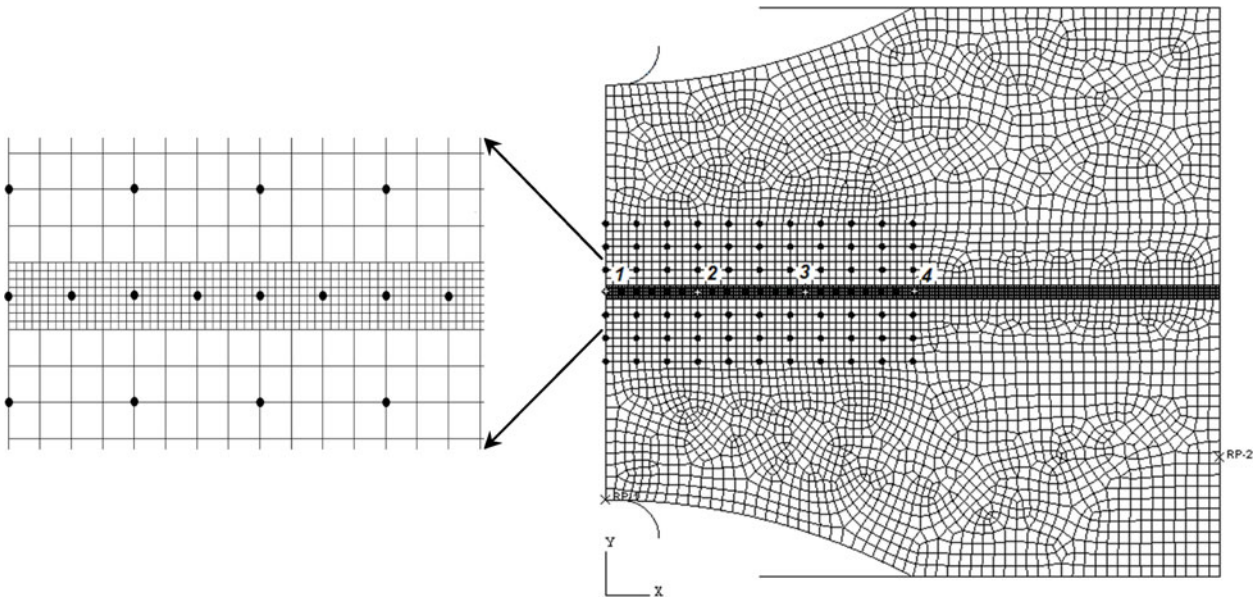

Fig. 2. Mesh for 2D finite element simulations, with nodes where displacements are measured by DIC (nodes 1, 2, 3, and 4 are selected for sensitivity assessment); the enlargement on the left specifies mesh and nodes locations in the specimen.

(d) In the lower block, or in both blocks, a groove can be prearranged for a possible crease in order to test the behavior of the paperboard under compression, with or without bending, orthogonal to a creasing line in it. Such prospect will be considered in future developments.
(e) As an alternative (not investigated in this article) to the above "soft" blocks, much stiffer blocks may be adopted and located at a suitably selected distance one from the other, so that the specimen inserted between them can be tested under compression with instability bending under control.

2.2. *Full-Field Measurements*

At each one of the steps within the rotation history planned for the test, many displacements have to be measured by a camera suitable to the DIC technique according to the criteria outlined in what follows. Details on DIC methodology, omitted here for brevity, are presented in a growing literature (e.g., in references [5–7] as for the peculiar features related to the present application).

The surface monitored by DIC is the one presented in Figure 1. The displacements due to the planned loading steps are measured by (now commercial) software that performs comparative analyses of the two photographs taken before and after the loading step on a preselected area, which is called "region of interest" (ROI) in the jargon employed in the relevant publications. The measurements concern material particles located before deformation in sub-areas around "nodes" selected among those of the FE model where displacements are computed. These sub-areas (called ZOIs, namely "zones of interest") are characterized by "gray levels," which permit to recognize the material particle after deformation and to quantify its displacements (the possible high number of resulting experimental data justifies the expression "full-field" displacements). The nodes considered in the numerical examples presented herein are visualized in Figure 2. Each ZOI corresponds to a set of "pixels" within a regular pixel grid pre-established in the camera over the ROI with such a high density (say 4000 × 4000 pixels), such that each one of the above nodes can be considered as coincident with a pixel with negligible possible errors.

Quantitative data of representative examples will be presented in Section 3. The following circumstances are of general interest in the present context of preliminary study: (i) nodes for displacement measurements should not be placed on the emerging interfaces between blocks and specimen; (ii) the sensitivity analysis methodology (e.g., [8–9], see Section 3) provides criteria for the nodes selection, which is governed also by DIC limitations [5]; (iii) negligible is possible mismatch between the nodes monitored by DIC and nodes of the finite element (FE) model, where displacements are computed by test simulations; (iv) in the test design, the preservation during the test of the original symmetry with respect to the middle vertical cross section (see Figure 1a) and the extension of the DIC monitored area (ROI) on both sides of the symmetry plane may lead to comparative assessment of intrinsic variability in the properties estimated and of possible inaccuracy of the test.

In the present context of numerical exercises for future equipment materialization, a 0.2 μm standard deviation is attributed to DIC experimental data, namely, minimal errors according to the present literature (see, e.g., [5, 6, 10]).

2.3. *Inverse Analysis Procedure*

The "sandwich system" envisaged and qualitatively described in Section 2.1 is clearly complex. In fact, it is inhomogeneous,

with three components: specimen, stabilizing blocks, and interfaces. Nonlinearities arise from possible large deformations and inelastic strains; dissipative and non-holonomic phenomena are expected within the specimen and on the unilateral contact interfaces. Obviously, accurate computer simulations are needed, and are here performed by a FE commercial code. However, substantial unusual requirements for computations arise in the present context. The computational efforts, to be carried out for each category of foils routinely tested in an industrial environment, are outlined below as operative stages according to the methodological novelties proposed in this article.

(a) Comparative simulations are preliminarily needed in order to design (by trial-and-error) the shape and dimensions of the sandwich test (ST) device for each category of foils and in order to perform sensitivity analyses apt to select the experimental data achievable by DIC.
(b) Comparative simulations of typical tests apt to check accuracy and to select acceptable approximations (in particular to move from 3D to 2D modeling) are useful in order to decrease computing cost of routine applications.
(c) As a preparatory phase (done once-for-all) of the proper orthogonal decomposition (POD) pointed out below in point (f), a test simulation has to be performed for each one of all the grid nodes preselected in the space of the sought parameters within the "search domain," suggested by an "expert" (i.e., by previous expertise).
(d) The POD procedure (outlined in the appendix) implies, as preparatory computation, the solution of an eigenvalue problem of a large matrix (order equal to double of the number of grid nodes) and consequent "compression" of the results ("snapshots") of phase (c).
(e) The inverse analysis leading from effects to causes here is deterministic, centered on the minimization, with respect to the sought parameters, of a "discrepancy function." This function, not necessarily convex, of the sought parameters and variables, quantifies the discrepancy between the experimental data (loading external actions and DIC measurements) and their counterparts computed as functions of the sought parameters. Such inverse analysis can be performed either by a mathematical programming algorithm (like here in Section 3) or by a "soft computing" technique (artificial neural network, like in [4] for cruciform tension tests, or genetic algorithm).
(f) Whatever of the above mentioned inverse analysis methods is adopted, it can be made fast, economical, and performable routinely by a small computer in real-life applications, by the exploitation of the preparatory POD results provided by the "a priori" computations of phases (c) and (d); in fact, a test simulation by interpolation of POD "compressed" results generally requires computing time of several orders-of-magnitude shorter than a FE simulation of the same test (see, e.g., [11–13]).
(g) Laminates consist of several plies with different mechanical properties, but their local behavior in terms of generalized variables (as plates or shells) are needed for overall structural analyses of products (such as liquid containers). Here a "fictitious homogeneous material" is considered for parameter identification in view of the subsequent fast "transition" to generalized variables, as described in Section 6.

3. Formulation of a Typical Foil Characterization Problem

3.1. *On the Foil Specimens to Test*

The rectangular specimen considered in what follows for parameters identification according to the proposed methodology exhibits the following features adopted for representative examples: thickness: $T = 0.46$ mm in the "Z direction" (according to the nomenclature usually employed in the paper industry), which is considered as Cartesian axis 3; length: $L = 40$ mm in the plane of imposed rotations and of DIC measurements; width: $W = 10$ mm orthogonal to that plane.

In the frequent presence of anisotropy, length and width of the sample are here assumed either coincident with the "machine direction" (MD), i.e., axis 1, and, respectively, with the "cross direction" (CD), i.e., axis 2; or, alternatively, coincident with exchanged principal directions (CD and MD) in subsequent tests. Thus, symmetry with respect to the central vertical plane holds during the test, with consequent simplifications in its modeling.

On the mechanical behavior of the specimen in the sandwich tests, the following hypotheses are assumed for the present preliminary investigations: homogeneity, even if the laminate to be tested clearly consists of plies with diverse materials (this basic assumption can be interpreted as recourse to a "fictitious material" attributed to the laminate); orthotropy (special case of anisotropy) with principal directions along axes 1, 2, and 3 above identified with directions MD, CD, and ZD, respectively, recurrent and meaningful in the paper and paperboard industry; elastoplasticity with isotropic hardening (absence of cyclic inelastic deformation makes irrelevant possible differences of hardening and possible damage in the sense of elastic stiffness reductions); positive definiteness and symmetry of the elastic stiffness matrix; plane stress states according to axes 1 and 3 (or 2 and 3), in view of the relatively small distance between the two vertical free surfaces of the system; finally, additivity of elastic and plastic strains in the "large strain" context considered in the commercial FE code and not examined herein, see e.g., [14].

According to the above assumptions, the following classical relationships describe the material model attributed to the foil under consideration (e.g., [15, 16]):

$$\begin{bmatrix} \varepsilon^e_{11} \\ \varepsilon^e_{33} \\ 2\varepsilon^e_{31} \end{bmatrix} = \begin{bmatrix} \frac{1}{E_{11}} & -\frac{\nu_{31}}{E_{33}} & 0 \\ -\frac{\nu_{13}}{E_{11}} & \frac{1}{E_{33}} & 0 \\ 0 & 0 & \frac{1}{G_{31}} \end{bmatrix} \underbrace{\begin{bmatrix} \sigma_{11} \\ \sigma_{33} \\ \sigma_{31} \end{bmatrix}}_{\sigma}, \qquad (1)$$

$$f = \sqrt{\boldsymbol{\sigma}^T \mathbf{Q}\, \boldsymbol{\sigma}} - \sigma_Y \le 0,$$

$$\mathbf{Q} = \begin{bmatrix} \frac{1}{R_{11}^2} & -\frac{1}{2}\left(\frac{1}{R_{11}^2} + \frac{1}{R_{33}^2} - \frac{1}{R_{22}^2}\right) & 0 \\ -\frac{1}{2}\left(\frac{1}{R_{11}^2} + \frac{1}{R_{33}^2} - \frac{1}{R_{22}^2}\right) & \frac{1}{R_{33}^2} & 0 \\ 0 & 0 & \frac{3}{R_{31}^2} \end{bmatrix}, \quad (2)$$

$$\dot{\boldsymbol{\varepsilon}}^p = \begin{bmatrix} \dot{\varepsilon}_{11}^p \\ \dot{\varepsilon}_{33}^p \\ 2\dot{\varepsilon}_{31}^p \end{bmatrix} = \dot{\lambda}\frac{df}{d\boldsymbol{\sigma}}, \quad f \le 0,\ \dot{\lambda} \ge 0,\ f\dot{\lambda} \ge 0, \quad (3)$$

$$\sigma_Y = \sigma_\infty - (\sigma_\infty - \sigma_0)\, e^{-n\,\varepsilon^p},$$
$$\text{where } \dot{\varepsilon}^p = \sqrt{(\dot{\boldsymbol{\varepsilon}}^p)^T \mathbf{Q}^{-1} \dot{\boldsymbol{\varepsilon}}^p}, \quad (4)$$

$$\dot{\varepsilon}_{ij} = \dot{\varepsilon}_{ij}^e + \dot{\varepsilon}_{ij}^p. \quad (5)$$

Hooke's law of orthotropic linear elasticity (Eq. (1)), in view of matrix symmetry, is governed by four parameters to which the following values (typical of paperboard for food containers) are assigned for subsequent numerical exercises by inverse analysis: Young moduli $E_{11} = 4300$ MPa, $E_{33} = 600$ MPa, shear modulus $G_{31} = 60$ MPa, $\nu_{13} = 0$. Parameter identifications will take account of the following constraints due to positive definiteness of the stiffness matrix in Eq. (1):

$$E_{11},\ E_{33},\ G_{31} > 0, \quad |\nu_{13}| < \sqrt{\frac{E_{11}}{E_{33}}}. \quad (6)$$

Hill's model of orthotropic plasticity (see, e.g., [15, 16]) is described by Eqs. (2)–(5) as follows: Eq. (2) defines the yield function f; Eq. (3) concerns the associativity of plastic strain rates and the complementarity relationship between yield function and plastic multiplier rate; Eq. (4) specifies isotropic hardening through an exponential relation between the current yield stress σ_Y and effective plastic strain ε_p, a relation which contains as parameters the initial yield limit σ_0, the asymptotic saturation stress σ_∞, and the hardening coefficient n. Finally, Eq. (5) evidences the strain additivity.

The values attributed herein to the seven parameters that quantify Eqs. (2)–(5) are as follows: $R_{11} = 1$, $R_{22} = 0.5$, $R_{33} = 0.5$, $R_{31} = 0.2$, $\sigma_0 = 30$ MPa, $\sigma_\infty = 70$ MPa, $n = 300$. These data are typical for the paper and paperboard industries and fulfill the loose inequality established in Ageno et al. [17].

It is worth noting that the traditional Hill model considered in this preliminary study of "sandwich" tests is calibrated here in view of its use for description of foil behavior under compression-dominant, noncyclic stress states. Other parameters estimates should be achieved and attributed to this model if different stress states, particularly if tension-dominant, are expected in the foil employment.

The advanced model proposed in Xia et al.[1] may be preferable in many industrial situations for paper, paperboard, and related products. However, it contains 27 parameters (reduced to 17 for the simplification and calibration by tension tests proposed in [4]); laminates for containers are primarily considered here under dominant compression. These circumstances have motivated reference to a classical plasticity model for the present study.

The interfaces between specimen and blocks and between blocks and rigid clamps are interpreted as loci with unilateral contacts and Coulomb friction without dilatancy. Therefore, the following interface model implemented in the commercial code Abaqus [18] is employed herein, denoting by p the pressure (normal stress, positive if compressive, on the interface):

$$f_c = |\sigma_{31}| - p\ \tan(\varphi) \le 0, \quad \dot{\gamma} = \dot{\lambda}\ sign(\sigma_{31}), \quad \dot{\lambda} \ge 0,$$
$$f_c\,\dot{\lambda} = 0. \quad (7)$$

Friction coefficient $\tan(\varphi) = 0.3$ is here assumed for all interfaces in the present preliminary investigations.

3.2. *A Representative Test and Its Computer Simulations*

The material of the "sandwich blocks," as mentioned in Section 2, must satisfy some obvious requirements, such as reversible isotropic elastic behavior during the test, and simplicity and economy for multiple block production. Among several polymers complying with the above needs, the one selected herein exhibits the following parameters in Eqs. (1) and (6) specialized to isotropy: $E_{11} = E_{22} = E_{33} = 6.0$ MPa, $\nu = 0.49$.

The geometry of the two blocks must be coherent with the geometry of the specimen; therefore, the horizontal surface, same for both blocks, is a rectangle with sides L and W and is a plane of symmetry before deformations.

The shape of the stabilizers in the vertical central plane of symmetry is governed by the three geometrical parameters: h, k, and α, as shown in Figure 1. Since the block profile between the clamps is assumed to be circular, these parameters are the main variables in the design of the sandwich system.

For the numerical exercise presented here in order to exemplify the proposed procedure, the following values are assumed: $h = 9$ mm, $k = 10$ mm, $\alpha h = 6.5$ mm ($\alpha \cong 0.72$), and $d = 4$ mm.

Preliminary computations (here omitted for brevity) have shown that these values are consistent with the category of paperboards considered now, a category with properties similar to those specified in Section 3.1 for a representative specimen.

As stated in Section 2.1, item (c), the measurement stages are defined in terms of clamps rotations corresponding to pre-selected photographs in the DIC sequence. Specifically, in the numerical exercises carried out in this preliminary study, the measurement stages are quantified as follows—rotations: 0.025, 0.05, 0.075, 0.10 radiants. The corresponding "shortenings" ($\Delta L/L$) are: 0.654, 1.308, 1.962 and 2.615%.

For the DIC measurements, the selected ROI (in the sense specified in Section 2) and the ZOIs in it are visualized in Figure 2 through the "nodes": 41 nodes along the specimen axis; 126 concerning the blocks. The 2D displacements in the surface will be experimental data for inverse analyses, account taken of the expected (and computationally predicted) symmetry in the test with respect to the central vertical transversal plane. Therefore, the input for inverse analyses will consist of 2×87 displacements at each one of four measurement stages (i.e., extracted from five DIC photographs).

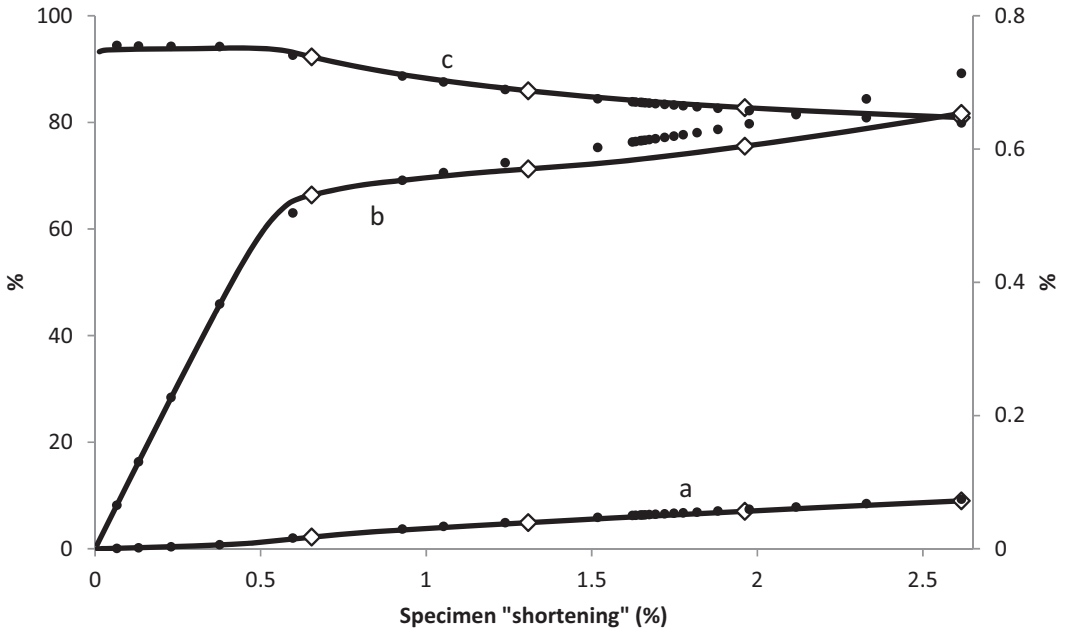

Fig. 3. Results of the test simulations with geometry shown in Figure 1 and features specified in the text: in abscissa is the percentage "shortening" of the specimen. The vertical displacement of the specimen central point (as percentage of the original specimen length) is visualized by plot (a), referred to ordinates on the left axis; the axial force on specimen in its central cross-section (as percentage of the total axial force in the central section of the sandwich) is shown by plot (b), left axis; plot (c) visualizes the average axial strain in central cross-section of the specimen, with reference to the axis on the right. Circular marks visualize the above results achieved by three-dimensional finite element modeling (see Subsection 4.1.); rhombs along each one of the three plots mark the four measurement stages.

Additional experimental data may concern the external action in terms of moment with respect to the rotation center (option (B) in (c), Section 2.1).

The commercial code ABAQUS is employed here in its 6.10-1 version [18]. The here adopted finite element (FE) discretization, with the mesh visualized in Figure 2, exhibits the following features: two dimensions in view of the assumed approximation of plane stress, 6300 finite elements with 2560 bi-linear elements on the specimen, and 1870 bi-linear elements on each stabilizing block. Such choice arises here from expertise on Abaqus use. Optimization of the FE modeling might be useful in future developments. The total number of degrees-of-freedom, including those concerning interfaces, amounts to 15,504.

In what follows the system dimensions and properties, which have been chosen in what precedes, are computationally checked by FE simulations ("direct analyses") of an experiment with compression and with bending as well. The sizes of blocks have been tentatively chosen in order to ensure controllable system behavior in testing and particularly to prevent specimen instability and bifurcations.

The centers of the opposite rotations imposed symmetrically to the rigid clamps are located 4.0 mm above the bottom surface of the lower block, as shown in Figure 1. The resulting main relationships are visualized in Figure 3. The specimen "shortening" (almost equal to average axial strain), represented as abscissa, means in percentage the horizontal relative displacement (i.e., distance reduction) between the two extreme cross sections (represented by their centroids) of the specimen. The intervals marked on the axis define the foreseen measurement steps.

4. Sensitivity Analyses

4.1. *Preliminary Remarks*

First the roles and consequences of some assumptions with "a priory" doubtful accuracy are investigated here below.

(a) In order to check the admissibility of the 2D interpretation of the system (plane stress hypothesis), the same compression and bending test in Subsection 3.2 is now simulated, with equal data, by means of a FE discretization with a 3D mesh and brick elements, by using the same code (ABAQUS 6.10-1, [18]). The mesh emerging on the monitored surface is a little coarser than the one which is shown in Figure 2 and was used for previous 2D analyses. Results achieved by 3D simulations are visualized by circular marks in Figure 3 for comparisons to the 2D results plotted there and specified in the caption. The maximum vertical displacement of the central node of ZOI turns out to be 2.6% higher than the value provided by the preceding 2D analysis. The shear stress σ_{32}, clearly everywhere null under the 2D assumptions, with 3D modeling reaches

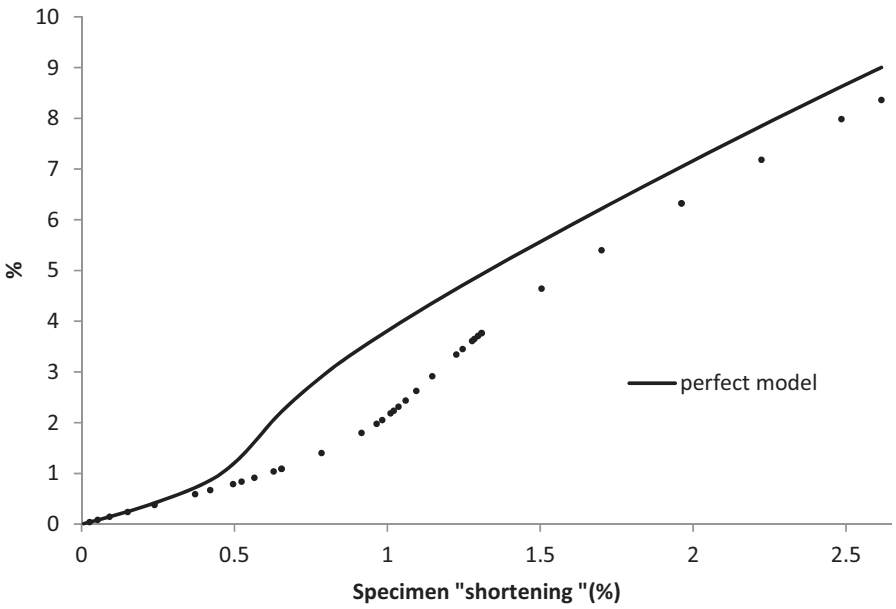

Fig. 4. Vertical displacement at the specimen center versus the specimen "shortening" in a test: circles quantify consequences of specimen length perturbation by −0.5%.

a maximum of 0.24 MPa, whereas the maximum shear in the bending plane of the specimen amounts to 2.42 MPa.

The above differences are acceptable to practical purposes, whereas the computing (CPU) times, with the same computer and same software, amounts to 50 s with 2D modeling and to 2250 s with 3D modeling. The above comparisons may justify in practice the simpler FE model adopted to the present purposes.

(b) Another numerical comparison specified here below concerns friction on the interfaces. While unilateral contact with Coulomb friction without dilatancy is regarded as fairly realistic, the coefficient $\tan(\varphi)$ can depend rather strongly on the specimen material and on the treatment of the foil surface during its production. Here, $\tan(\varphi) = 0.3$ is assumed on all interfaces for test simulations based on the same data considered in Subsection 3.2. The effects of friction change from $\tan(\varphi) = 0.3$ to $\tan(\varphi) = 0.4$ on the results above considered have turned out to be less than 3.8% for vertical displacements, 2.2% for average strains, and 0.4% for axial force. Errors in measured quantities due to errors in friction turn out to have consequences on the parameters estimates. Therefore, friction coefficient might be another parameter to identify. However, it is not estimated in the present preliminary numerical exercises of inverse analysis, also in view of the circumstance that, for the considered category of containers laminates, friction can be assessed fairly accurately in the factory by practitioners.

(c) The extraction by cutting of a specimen from the laminate to test may involve some inevitable inaccuracy. Test simulations by assuming specimen length L perturbed by -0.5% with respect to the clamps distance (possibly due to cutting inaccuracy) has led to a difference of 3.4% in the maximum loading force on the specimen and of 7.1% in the maximum vertical displacement at the specimen midspan, whereas this difference reaches 37% in some mid-stages of loading. Figure 4 visualizes the whole history of the vertical displacement and of the influence on it by the above perturbation on L. Therefore, as shown in the preliminary design sketch of Figure 1a, the foil sample is grasped by both symmetric rigid clamps; their distance before rotations equals the tested length L in the specimen, the length of which must be larger than L. Numerical exercises have shown that the stress localizations due to the grasping give rise to negligible deviations from the simulation results achievable by imposing at the ends of the interval L same boundary conditions for blocks and specimen (i.e., frictional contact with a rotating rigid wall).

(d) The last numerical check considered here concerns the self-weight of blocks, specimen, and belt. The self-weight turns out to be irrelevant as for all measurable quantities (displacements due to imposed rotations on clamps) used for parameter identification. The consequences of self-weight are only due to the preliminary stress state and, hence, are negligible and not considered herein, even if accounting for self-weight does not increase computing effort for test simulation.

4.2. *Formulation and Results*

Sensitivity analysis, in its traditional role, means assessment of the influence of a sought parameter on a measurable quantity (see, e.g., [8] in general, [4, 17, 19] for specific applications). The measurable quantities for the present mechanical characterization purposes are selected as follows: horizontal and vertical displacements of the nodes in the grid specified in Figure 2, along the specimen axis with double density with

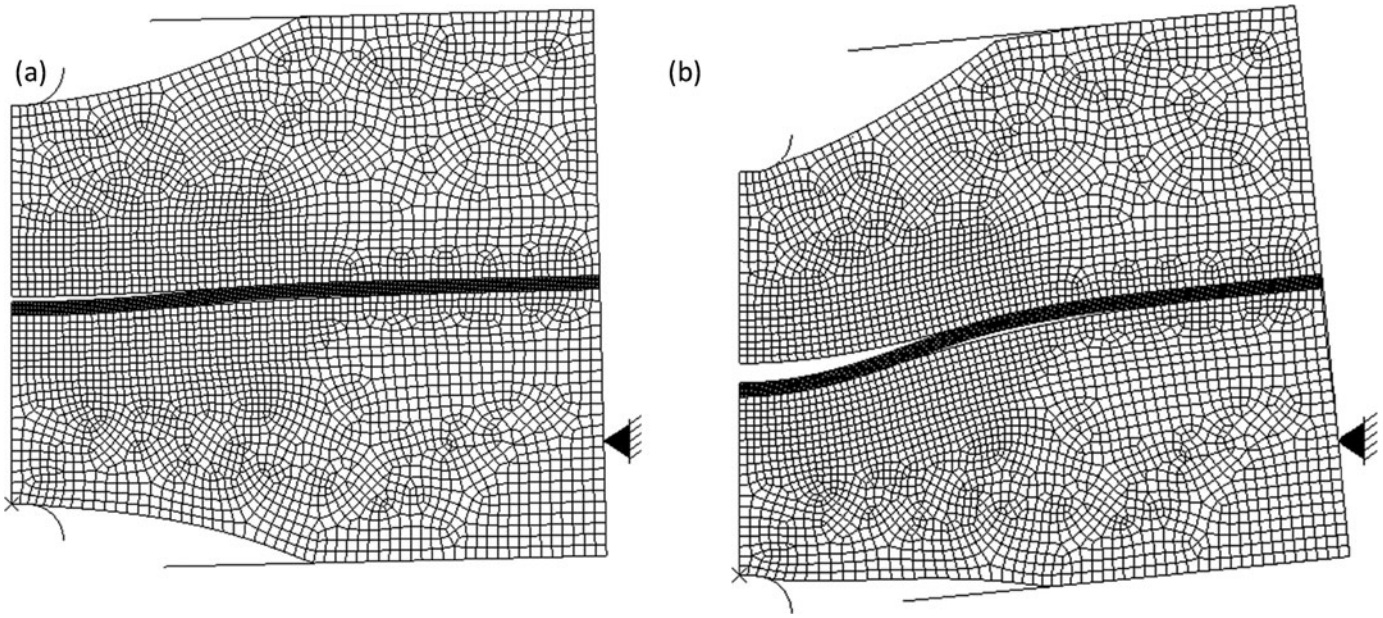

Fig. 5. Deformed configuration at the second (a) and final (b) measurement stage along the test described in Section 4.2.

respect to the near areas on the blocks. The measurements are supposed to be performed by DIC instruments now available on the market. Such experimental data may be supplemented by those on external actions according to option (B) in (c), Subsection 2.1.

The above displacements are extracted by five digitalized DIC photographs: before the test ($\Delta L = 0$) and at the end of each loading interval, namely, at shortenings $\Delta L/L = 0.654$, 1.308, 1.962, and 2.615%. These four measurement stages are marked by rhombs on the abscissa of Figure 3.

Figures 5a and 5b show the sandwich deformed configurations at the second and fifth (final) of the above specified stages. The latter figure evidences a remarkable detachment between specimen and upper block despite the stiffness of the central belt.

Traditionally, sensitivity is quantified by the partial derivative (here approximated by forward finite difference) of the measurable quantity as function of the parameter considered, function computed with the reference values attributed to all parameters. The reference values of all material model parameters are those specified in Subsection 3.1.

The following meaningful representative measurable quantities are considered here, namely, the horizontal and vertical displacements (positive if directed to the left direction and downward, respectively) in the DIC nodes 1, 2, 3, and 4 specified in Figure 2, the moment per unit "depth" in the transversal direction of the specimen (hence in N), as representative external action on the sandwich, all at the final stage of the test.

The parameters considered henceforth are those selected within Hill model in Section 3, namely, those listed here followed by the relevant reference values: elastic moduli E_{33} and G_{31}, yield limit σ_0, ultimate stress σ_∞ (600, 60, 30, 70 MPa, respectively); Poisson ratio ν_{13}, coefficient R_{31}, hardening exponent n (0, 0.2, 300, respectively).

For each parameter, preceding expertise on the technological processes suggests an interval to which the search can be confined (this information will be used also for the application of POD in Section 5 and in the appendix). To the present purposes, upper and lower bounds of the intervals conjectured for the parameters are those specified in the first row of Table 1. Their averages coincide with the reference values.

The following numerical exercises have been performed in order to achieve orientations for the inverse analysis strategy: (a) A single parameter p_i, each one in turn, is given its conjectured upper bound $p_i^{\max}$, while the other parameters are kept at their reference values. Then all representative measurable quantities u_h are computed by a FE simulation of the test (direct analysis); then similar direct analysis is carried out with the parameter at its conjectured lower bound $p_i^{\min}$. (b) The difference $u_h(p_i^{\max}) - u_h(p_i^{\min})$ between the two above values resulting for each one of the preselected measurable quantities u_h are compared to a quantification of the inaccuracy expected in the relevant measurement (e.g., the standard deviation of the adopted instrument). (c) If the former is sufficiently larger than the latter value (say by one or two orders of magnitude), the identifiability of the considered parameter can be reasonably expected.

The peculiar criterion of sensitivity analysis above adopted (instead of the popular one based on normalized derivatives) has led to Table 1.

A typical representative inaccuracy of 0.2 μm might be attributed to experimental data provided by DIC in the present context (see, e.g., [5, 6]). The inaccuracy of the load measurements cannot be quantified at the present preliminary stage of design.

Numerical results like those outlined in what precedes and other qualitative considerations have led to the following conclusions as for the parameter estimation.

Table 1. Intervals of horizontal (first in each cell) and vertical displacements (in μm, positive directions left and downward) of representative nodes and (last row) of loading moment (in N, per unit depth), corresponding to intervals conjectured by expert for the material parameters

		Parameters and relevant conjectured intervals						
Measurable quantity	Nodes	E_{33} [MPa] 400–800	ν_{13} −0.02–0.02	G_{31} [MPa] 40–80	σ_0 [MPa] 20–40	σ_∞ [MPa] 50–90	n 200–400	R_{31} 0.1–0.3
Displacements [μm]	1	0.00	0.00	0.00	0.00	0.00	0.00	0.00
		−0.64	1.15	31.25	59.45	−35.42	14.31	38.87
	2	−0.11	0.03	2.51	3.68	−24.53	−1.95	4.08
		0.12	0.49	13.78	32.75	66.96	16.21	14.63
	3	−0.22	−0.01	−9.69	−2.16	−33.18	−6.88	−11.14
		0.62	0.64	50.22	41.88	99.05	30.38	51.13
	4	−0.04	−0.06	−6.31	−3.76	−2.44	−2.73	−4.03
		0.09	0.69	31.21	37.93	−19.15	10.89	21.66
Load [N]	—	0.011	0.005	−0.336	−0.294	1.228	0.089	−0.408

Elasticity moduli do not need to be estimated in the present procedure: those in the foil plane (E_{11}, E_{22}, G_{12}, and ν_{12}) are generally supposed, in practice, not significantly changed from tension- to compression-dominated stress states and, therefore, can be identified by tensile cruciform tests popular in engineering practice (see, e.g., [4, 19]); in the thickness direction, three simple compression tests provide economically the elastic moduli E_{33}, G_{31}, and ν_{31}, while G_{32} and ν_{32} are obviously immaterial for the present experiment, which can be considered in plane-stress state (see preceding Subsection 4.1).

Among the plasticity parameters, R_{31} is here a priori assumed $R_{31} = 0.2$ according to the usual assumption in the present industrial practice (without inverse analyses), since the shear stress σ_{31} is expected to be relatively small in "sandwich tests." Also, normal stress σ_{33} in thickness direction clearly turns out to be small in such testing and, hence, to the relevant parameter R_{33} the value 0.5 is here attributed, like usually so far in industrial environment. The Hill moduli R_{22} and R_{33} are immaterial to the present purposes because the normal stress $\sigma_{22} = 0$ consistently with the two-dimensionality assumptions and σ_{33} can be regarded as negligible in sandwich tests, as evidenced by Eq. (2); $R_{11} = 1$ is implied by Hill's Eqs. (2) and (4) since at the yield onset, in a hypothetical uni-axial test, $f = 0$ implies that $\sigma_{11} = \sigma_Y = \sigma_0$. Clearly, all non-dimensional parameters $R_{ij} = 1$ in isotropy.

In the Hill model, the symmetry of the yield criterion with respect to the stress origin and the here assumed isotropic hardening law can be employed to describe the fictitious material assumed for the laminate to characterize because no reverse stress is involved in the sandwich test under consideration.

As a conclusion, the parameters to estimate in the present context are three: the initial yield stress σ_0; the asymptotic ultimate stress σ_∞; and the hardening coefficient n. The sensitivity analyses, which led to Table 1, permit to foresee the identifiability of these parameters by means of the proposed sandwich test with compression on the foil specimen.

5. Parameter Estimation by Mathematical Programming

5.1. *Inverse Analysis Procedure*

The same FE simulations performed in what precedes for "direct analyses" of a test with bending and compression combined, will be repeatedly employed in what follows with suitable sequences of parameter vectors for "inverse analysis."

The two inverse analysis procedures employed herein are at present well known in the applied mathematics community and described in the literature; therefore, a brief survey of both is relegated to the appendix, whereas references [12, 13, 20–22] are cited as sources of detailed information.

The present deterministic approach to parameter identification rests on the minimization of the "discrepancy function" (DF) ω, which can be formulated as follows:

$$\omega_{\min} = \min_{\mathbf{p}} \{\omega(\mathbf{p}) = [\bar{\mathbf{u}} - \mathbf{u}(\mathbf{p})]^T \mathbf{C}^{-1} [\bar{\mathbf{u}} - \mathbf{u}(\mathbf{p})]\}. \qquad (8)$$

In the above formulation: the N-vector $\bar{\mathbf{u}}$ gathers the experimental (here "pseudo-experimental") data and vector $\mathbf{u}$ their counterparts computed as functions of the sought parameters (variable vector $\mathbf{p}$); $\boldsymbol{C}$ is the covariance matrix, which quantifies the random errors in the measurements provided by the adopted instruments and attributes, by its inverse, role to more accurate data. Here, the identity matrix is assumed as $\boldsymbol{C}$ in the absence of true experiments and in view of the irrelevance of such features to the present purposes of preliminary analysis on methodological innovations in structural diagnosis of foils.

"Pseudo-experimental data" means measurable quantities computed on the basis of selected values attributed to the sought parameters and later used to check the accuracy of the estimates resulting from the inverse analysis. The discrepancy function $\omega(\mathbf{p})$ turns out to be nonlinear and not necessarily a convex function of the variable parameter vector $\mathbf{p}$; therefore, it might exhibit local minima and lack of uniqueness of the absolute minimum. The minimization of the DF is performed

here by nonlinear mathematical programming, comparatively with the following two procedures, quite different from the standpoint of practical applications. Both are briefly outlined in the appendix with references for details.

(a) Trust region algorithm (TRA): from an initialization by reasonable values attributed to the sought parameters, up to convergence; in each iteration step a two-variables quadratic programming problem is formulated by means of only first-derivatives (approximated by finite differences) of the function ω to minimize.
(b) Proper orthogonal decomposition (POD), which requires, as already pointed out in Sec.2.3, preliminary "direct analyses" based on parameter vectors defined by nodes preselected in the parameter space within the "search domain" defined by an "expert" on the basis of the previous expertise (here by lower and upper bound for each parameter to identify); after these (numerous) usual FE simulations, the so-called "compression" of the results ("snapshots") is carried out, and any other test simulation can be achieved in a very fast way by interpolations through radial basis functions (RBF); therefore, due to the preparatory works, the minimization of the $\omega(\mathbf{p})$ by the above mentioned TRA becomes very economical in terms of computing times and the size of the computer.

Clearly in the real-life simulations, procedure (b), say POD + RBF + TRA, is preferable and often strongly advantageous when parameters estimation has to be performed frequently and routinely, in an "ad hoc" laboratory.

In view of possible local non-convexity in the objective function $\omega(\mathbf{p})$ (and, hence, possible convergence to a local minimum), the reliability of the estimates $\bar{\mathbf{p}}$ achieved after TRA convergence (according to a suitable criterion, see,e.g., [20, 21]) can be checked by some "ad hoc" criterion, such as minimization repeated with diverse initializations; minimum eigenvalue of the approximated Hessian at $\bar{p}$ to assess convexity of ω; and assessment of the achieved $\omega_{\min}$ as compatible with accumulation of round-off errors along the iteration sequence.

5.2. *Calibration of a Homogeneous Material Model by a Test with Combined Compression and Bending*

The "a priori" known data concerning the sandwich system designed in the preceding sections are adopted for the inverse analysis exercises that follow. The parameters to estimate within the Hill model specified in Section 3 are those selected in Section 4, namely, the initial yield stress σ_0, the maximum stress σ_∞ (asymptotic saturation stress), and hardening coefficient n. Other parameters have turned out in what precedes to have negligible influence on measurable quantities in the experiment and/or to be a priori assessed; to these parameters reasonable values have been attributed according to the previous expertise (see Section 3).

Along the loading process of the external action consisting of equal opposite rotations imposed on the two rigid clamps, the four preselected measurement steps correspond to specimen "shortenings": 0.654, 1.308, 1.962, and 2.615%. The pseudo-experimental data considered as input of the inverse analysis are chosen according to the following alternatives: (A) the vertical and horizontal displacements measured by DIC on the ZOI located on the specimen, as shown in Section 3 (two displacements in each of 87 DIC grid nodes, Figure 2, at each one of the four measurement stages, $N = 696$ data altogether); (B) these same data enriched by the four measurements of the moment loading the sandwich.

The two mathematical procedures mentioned in the preceding subsection (and outlined in the appendix) have been comparatively applied.

The main results are presented in what follows.

(a) The parameter identification by TRA is illustrated in Figure 6 for two different initializations. The values of the sought parameters at each step along the TRA procedure are expressed in percentage of their "actual values" employed for the "a priori" computation of the pseudo-experimental data.

    The TRA employed here in the inverse analysis exercises for validation of the new method is implemented in MATLAB 7.9.0 [23, 24] and described in references [20, 21] with a convergence criterion mentioned in the appendix, and quantified here with the choice of 10^{-8} as the value considered equivalent to zero for the assessments of the discrepancy function minimum. The plots in Figure 6a and 6b visualize TRA convergence without and with moment measurements in the inverse analysis input, i.e., with the above alternative (A) and (B), respectively. Such comparisons evidence desirable advantages of alternative (B) in the experiment. The (CPU) computing time to reach that minimum, with the computer (same as the one employed in Section 3), has amounted to about 2 h with both initializations.
(b) Now the same estimation problem is tackled by the POD + RBF + TRA procedure [12, 13, 23, 25]. The chosen search domain is a parallelepiped in the three-dimensional space of the sought parameters, with edges defined by their conjectured intervals (Section 4.2, Table 1). The grid on this domain is generated by assuming nine nodes equally spaced along each axis. Matrix $\mathbf{U}$ (see appendix) consists of: $M = 9^3 = 729$ "snapshots," each one being a vector of $N = 696 + 4$ pseudo-experimental data.

The 40 larger eigenvalues among the $N = 696 + 4$ not a-priori null eigenvalues λ of matrix $\mathbf{D} = \mathbf{U}^{\mathrm{T}}\mathbf{U}$ are plotted in Figure 7. Truncation is performed after $\lambda = 8.8\text{e-}5$, thus generating a "truncated basis" for "reduced amplitudes" with dimensions $\hat{N} = 20$. For the interpolations, the radial basis functions (RBF) [22] chosen here are:

$$g_i(\mathbf{p}) = (\|\mathbf{p} - \mathbf{p}_i\|^2 + r^2)^{-1}, \quad i = 1, 2, ..., 729, \tag{9}$$

where $\mathbf{p}$ is the variable parameter vector and $\mathbf{p}_i$ is the vector in node i within the grid over the search domain; to the "smoothing coefficient" r the value $r = 0.74$ is attributed here according to the criteria explained, e.g., in [22, 21].

By exploiting the above POD + RBF preparatory work for abbreviated test simulations (instead of further laborious

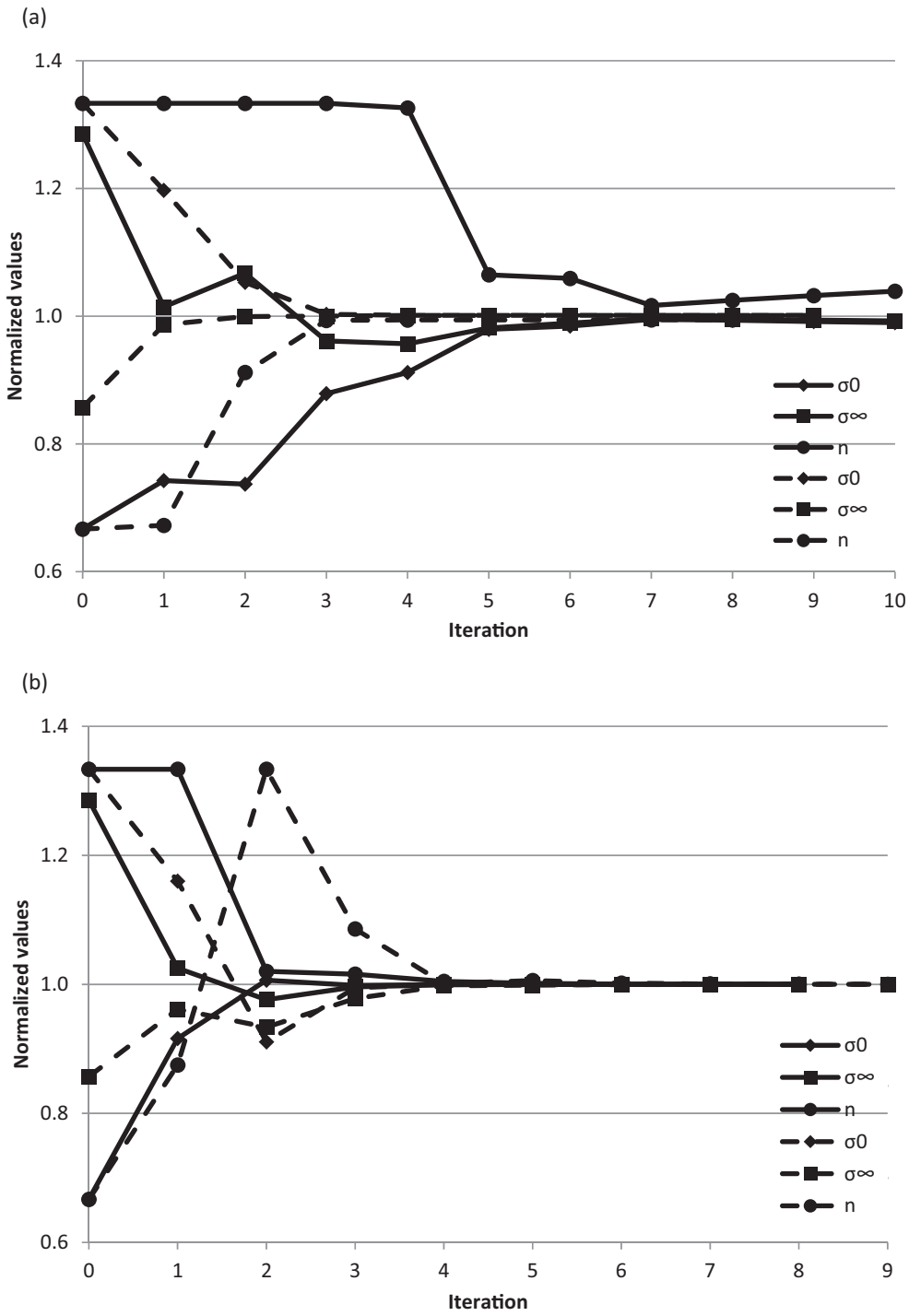

Fig. 6. Convergence of TRA for the estimation of parameters by the compression and bending test designed in what precedes: solid lines initialized with $[\sigma_0, \sigma_\infty, n] = [20, 90, 400]$ and dashed lines initialized with $[\sigma_0, \sigma_\infty, n] = [40, 60, 200]$. (a) Pseudo-experimental data concern DIC measurements of node displacements only. (b) The four loading data are exploited as well.

FE modeling), TRA has been applied on the very same context by the same initializations. The estimates achieved by the two above adopted computational procedures turned out to exhibit differences of -0.01, -0.01, and 0.00% for the parameters σ_0, σ_∞, and n, respectively.

It is particularly meaningful for practical applications to compare the following computing time: (a) 1:45 h by TRA above; (b) the procedures POD + RBF + TRA required 31 h for the preparatory efforts by FE simulations and only 0.9 s for the parameter estimation. The computer employed has been again the same indicated in Section 3.

The transition from a node belonging to the training grid to a point out of that grid may have, on the estimates, consequences that have been checked as follows.

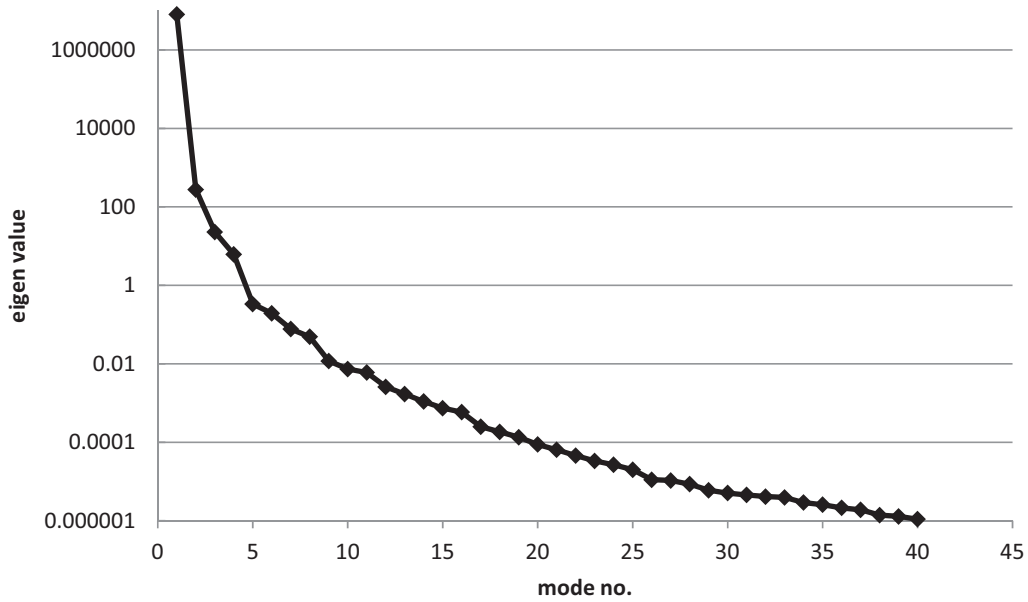

Fig. 7. The sequence of non-zero eigenvalues of matrix D in descending order.

Let the no-grid point be $[\sigma_0, \sigma_\infty, n] = [36, 62, 260]$ (quite far from the eight vertices of a grid cell); the very same POD + RBF + TRA procedure has led to estimates affected by the following errors: 2.3% as for exponent "n"; less than 0.6% for the other two parameters.

The other simplifying transition from 3D to 2D finite element modeling clearly implies errors in parameter estimation, besides the test simulation. Some checks have been made on such inaccuracies for the two points in parameters space $[\sigma_0, \sigma_\infty, n] = [30, 70, 300]$ and $[\sigma_0, \sigma_\infty, n] = [36, 62, 260]$ with the following representative results, again with the modeling differences specified at point (a) in Section 4.1. 1.95% as for the initial yield limit σ_0, 1.45% as for the asymptotic saturation stress σ_∞, and 4.16% as for hardening exponent "n".

Finally, some numerical exercises have shown that errors in experimental data imply inaccuracies for not-larger order of magnitude in the parameter estimates. The pseudo-experimental data set for alternative (B), i.e., including moments, has been generated 50 times and perturbed by random addends with uniform probability density over the interval $\pm$ 1 μm for the displacements and $\pm$ 0.01 N for the external action. The consequent perturbations quantified by standard deviations in the results of the POD + RBF + TRA procedure turned out to be $-0.20 \sim +0.18$ MPa ($-0.65\% \sim +0.59\%$), ± 0.67 MPa ($\pm 0.96\%$), and $-11.25 \sim +14.10$ ($-3.75\% \sim +4.70\%$) on σ_0, σ_∞, and n, respectively; namely, as expected larger for the hardening coefficient than for stress limits.

6. Calibration of a Generalized Variables Model

6.1. *Preliminary Remarks*

What precedes has concerned the design of the "sandwich system" and preliminary orientative computational exercises on its use for characterization of the behavior of foils or laminates in the presence of compression. In that preparatory stage, the specimen has been assumed as a homogeneous solid and was discretized by FE as such (in two or three dimensions) like the surrounding "blocks" which stabilize it. For laminates, paperboards, and other kinds of foils to be used in industrial products (like boxes and containers), the mechanical models of practical interest are in "generalized variables," namely, in bending moments, axial forces, shear forces (per unit length in the foil plane), and corresponding kinematic variables. Therefore, the behaviors of foils as beams or plates, not as solid continua, are to be modeled and calibrated. To such purposes two approaches can be adopted:

(i) after inverse analysis of the specimen as solid continuum, a consequent calibration is performed of a model in generalized variables;
(ii) different FE discretizations of the sandwich system are adopted, namely, the stabilizing "blocks" are discretized as continua but the specimen is modeled as a plate or beam.

The approach (ii), with the FE discretization of the specimen consistent with its interpretation as beam or plate, obviously implies that only such constitutive model, in generalized variables, has to be calibrated. The combination of diverse finite elements is implemented in some commercial codes (e.g., those oriented to geotechnical engineering, in view of recurrent situations with foundation beams or plates interacting with underlying soil to be considered obviously as a continuum).

The homogeneity assumption (i) as a continuum for the specimen material (which thus becomes "fictitious") requires recourse to a second (much simpler) parameter identification formulated in the subsequent subsection. However, it is

justified by the following motivations and, hence, it was adopted herein.

(a) Most paperboards and laminates are generated by production processes, which influence or determine in a practically unpredictable fashion the local properties of the various layers (namely, e.g., paper, aluminum, polyethylene) and relevant adhesions. Therefore, traditional homogenization procedures, popular for composites, are usually unreliable in the present industrial context.
(b) Commercial FE computer codes, like Abaqus adopted here, may lack software for modeling structures (like the present sandwich system) partly as 2D or 3D solid continua (here the "blocks") and partly as beams (here the laminate specimen), interacting through unilateral frictional contact. The elastic-plastic behavior of a beam in generalized variables, by such commercial code, would require the generation of "ad hoc" routines, possibly to be done for future applications.
(c) The specimen responses to the present "sandwich tests" are governed by the specimen behavior as a beam, namely, in terms of "generalized variables" and relevant parameters. As a consequence, the local properties of the individual plies in the laminate influence the overall deformed configuration of the specimen (i.e., the DIC measurable quantities) only through averages and are not quantifiable locally by computer simulations. Therefore, particularly if the laminate exhibits symmetry across thickness with respect to the middle plane (as assumed herein) the assumption of a "fictitious" homogeneous material as an intermediate step towards generalized models calibrations reflects the substantial feature of the test and do not jeopardize the final results (except, of course, through further round-off errors and approximations implied by the extended computational procedure).

6.2. *Transition from a Fictitious Material Model to a Model in Generalized Variables*

Let the purpose of the inverse analysis be now the calibration of a simple customary elastic-plastic-hardening model concerning local bending-compression of the foil specimen interpreted as a beam. Reference is made here to an usual nonlinear relationship, which relates bending moment M and axial force N as generalized stresses, to curvature γ and axial strain η as generalized strains (both being summations of elastic and plastic addends). With compact notation this "beam model", governed by new parameters gathered in vector $\mathbf{P}$, can be described by the formula:

$$\{N,\, M\}^T = \mathbf{f}\,(\mathbf{P},\, \eta,\, \gamma)\,. \tag{10}$$

The above relationship to the present purpose can be supposed to be history-independent (holonomic) since, specifically, a linear path from the origin without unloading is here considered in the plane of generalized strains η and γ, leading to the corresponding generalized stresses N and M.

Calibration of model (10) means that the parameters contained in it, say "generalized parameters" gathered in vector $\mathbf{P}$, have to be identified.

The inverse analysis carried out according to the procedures described in the preceding sections (i.e., based on the assumption of specimen as a homogeneous solid and on FE discretization as such) has calibrated the selected model $\boldsymbol{\sigma}(\boldsymbol{\varepsilon})$ of a "fictitious material" (fictitious if the foil is an inhomogeneous laminate). Such a model is adopted since it is judged to be apt to describe the overall deformation process that occurred in the specimen during the test and of the final products in service.

Let $\bar{}\alpha_i$ and $\bar{\gamma}_i$ represent a chosen pair of kinematic generalized variables, which define deformations at a beam cross-section. The calibrated model $\boldsymbol{\sigma}(\boldsymbol{\varepsilon})$ of the fictitious material leads, through a trivial computation (beam cross-section is rectangular), to the static generalized variables $\bar{N}_i$ and $\bar{M}_i$ corresponding to the above selected kinematic ones. The adopted beam model to calibrate provides static generalized variables corresponding to the chosen kinematic ones $\bar{}\alpha_i$ and $\bar{\gamma}_i$ through the parameters included in the unknown parameter vector $\mathbf{P}$. Therefore, the sought parameters governing the beam model can be estimated by solving (e.g., by TRA like in Section 5) the following simple inverse analysis problem consisting of minimization of a new discrepancy function Ω, namely:

$$\Omega_{\min} = \min_{\mathbf{P}} \Omega\,(\mathbf{P}) = \sum_{i=1}^{n} \left\| \left\{ \bar{N}_i,\, \bar{M}_i \right\}^T - \mathbf{f}\,(\mathbf{P}; \bar{\eta}_i,\, \bar{\gamma}_i) \right\|^2, \tag{11}$$

where $\|\|$ denotes Euclidean norm and n is the number of points to be chosen in the plane of kinematic variables η and γ, points whose number and locations must be selected in order to ensure well-posedness of the optimization problem and convexity of the discrepancy function Ω.

An application for validation of approach (i), presented above in Section 6.1, leading to the above second parameter identification, Eqs. (10) and (11), is developed as a simple example in what follows.

The model in generalized variables N, M considered here for preliminary numerical examples reads (see, e.g., [15, 16]), N being assumed positive in compression:

$$f_g = \frac{|M|}{M_Y} + \frac{N^2}{N_Y^2} - 1 \le 0, \quad TN_Y = \alpha M_Y, \tag{12}$$

$$M_Y = M_\infty - (M_\infty - M_0)\, e^{-\kappa \lambda_g}, \tag{13}$$

$$\dot{\eta}^p = \dot{\lambda}_g \frac{\partial f_g}{\partial N}, \quad \dot{\gamma}^p = \dot{\lambda}_g \frac{\partial f_g}{\partial M}, \quad f_g \le 0, \quad \dot{\lambda}_g \ge 0,$$

$$f_g\, \dot{\lambda}_g = 0, \tag{14}$$

$$\begin{Bmatrix} N \\ M \end{Bmatrix} = \begin{bmatrix} C_N & 0 \\ 0 & C_M \end{bmatrix} \begin{Bmatrix} \eta^e \\ \gamma^e \end{Bmatrix}, \tag{15}$$

$$\dot{\gamma} = \dot{\gamma}^e + \dot{\gamma}^p, \quad \dot{\eta} = \dot{\eta}^e + \dot{\eta}^p. \tag{16}$$

The meanings of the symbols are as follows: current yield limits N_Y, M_Y; elastic stiffnesses C_M, C_N; κ isotropic hardening coefficient; f_g and $\dot{\lambda}_g$ yield function and plastic flow multiplier, respectively; T is the foil sample thickness. Shear deformations are assumed to be negligible.

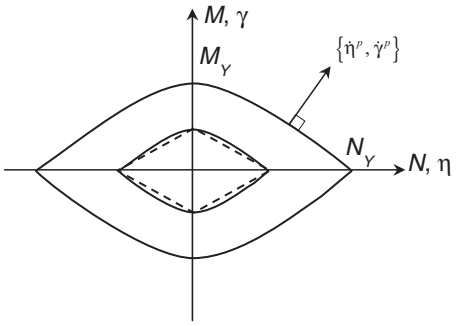

Fig. 8. Initial and ultimate parabolic yield surfaces (continuous lines) according to the generalized variables model; dashed straight lines show the initial yield surface according to Hill model, Eqs. (2)–(4).

The above classical and popular simple model of associative elastic-plastic-hardening beam behavior, attributed in direction MD (or CD) to the laminate specimen under testing, contains the following parameters to identify: C_N, C_M, M_0, M_∞, α, and κ. The variable yield limits N_Y and M_Y depend on the four plastic parameters through Eqs. (12) and (13). Figure 8 visualizes, according to Eqs. (12) and (13), the parabolic ultimate yield surface with $\lambda_g \to \infty$ and the initial one with $\lambda_g = 0$. The initial yield surface consistent with the Hill model, Eqs. (2)–(4), and with the homogeneity of the assumed "fictitious" material in the specimen is a rhomb (dashed lines in Figure 8).

6.3. *Comparative Numerical Exercises*

For some computational checks apt to validate the procedure leading to the calibration of the adopted generalized variables model, Eqs. (10)−(16), the following set of strain pairs $\bar{\eta}_i$, $\bar{\gamma}_i$ is considered; five radial straight lines are selected in the η, γ plane, namely:

$$\gamma\, T = \eta\, \tan(\beta)\,, \tag{17}$$

with angle β specified in Figure 9 and in subsequent figures; along each one of these lines, 1000 points (besides the origin) are considered at equal intervals (clearly, a sequence of growing strains along a radial line implies no unloading); the 1000 pairs $(\bar{\eta}_i, \bar{\gamma}_i)$ thus generated have been employed in the following two ways.

(A) For each sectional deformation $\bar{\eta}_i$, $\bar{\gamma}_i$ of the specimen, the generalized stresses N_i, M_i are computed using the Hill model calibrated for the fictitious homogeneous material in Section 5. Such trivial computations lead to results visualized by dashed plots in Figures 9 and 10.

(B) Solid lines in Figures 9 and 10 visualize results achieved by the following alternative computations: (a) all the above strain pairs $\bar{\eta}_i$, $\bar{\gamma}_i$ and the corresponding stress pairs $\bar{N}_i$, $\bar{M}_i$ are input into problem (11), where function **f** is defined by the constitutive model Eqs. (12)−(16); (b) the parameters in the variable vector **P** are those specified in the preceding subsection and are estimated by minimization (11) using once again the TRA algorithm; (c) finally, the calibrated model (12)−(16) is employed to generate generalized stresses on the basis of the same generalized strain pairs $\bar{\eta}_i$, $\bar{\gamma}_i$ earlier selected and above used in the starting stage (a); these new sequences of stresses $\bar{N}_i$, $\bar{M}_i$ corresponding to the same earlier selected strains $\bar{\eta}_i$, $\bar{\gamma}_i$ have led to the solid lines in Figures 9 and 10. The values of the estimated parameters are the following ones: $C_N = 2491$ N/mm, $C_M = 37.5$ N mm, $M_0 = 1.81$ N, $M_\infty = 3.66$ N, $\kappa = 9.54$, and $\alpha = 4.03$.

It is worth noting that, according to the rectangular shape of the cross-section and the homogeneous assumption on the constitutive model, the following quantities can be easily

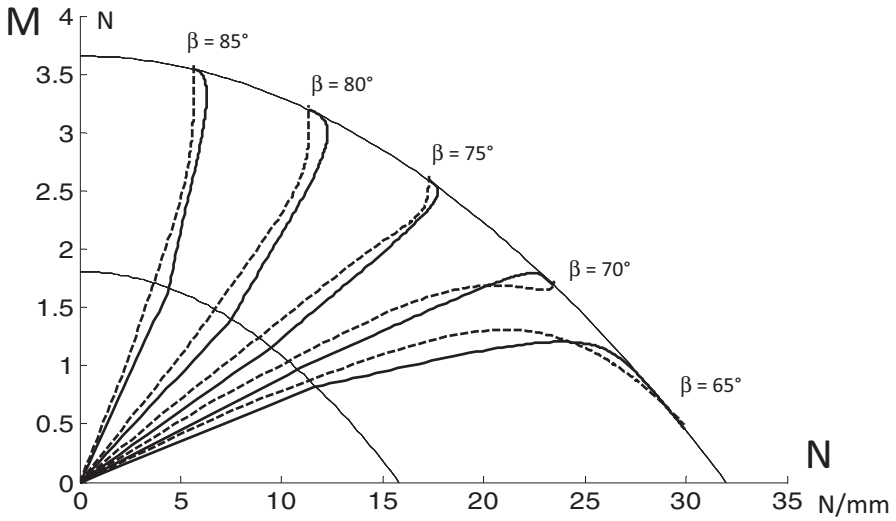

Fig. 9. Behaviors of the specimen cross section orthogonal to MD under imposed generalized strains η and γ along radial paths $\gamma\ T = \eta \tan(\beta)$: according to the calibrated generalized variables model (solid lines); according to the earlier calibrated continuum model (dashed lines).

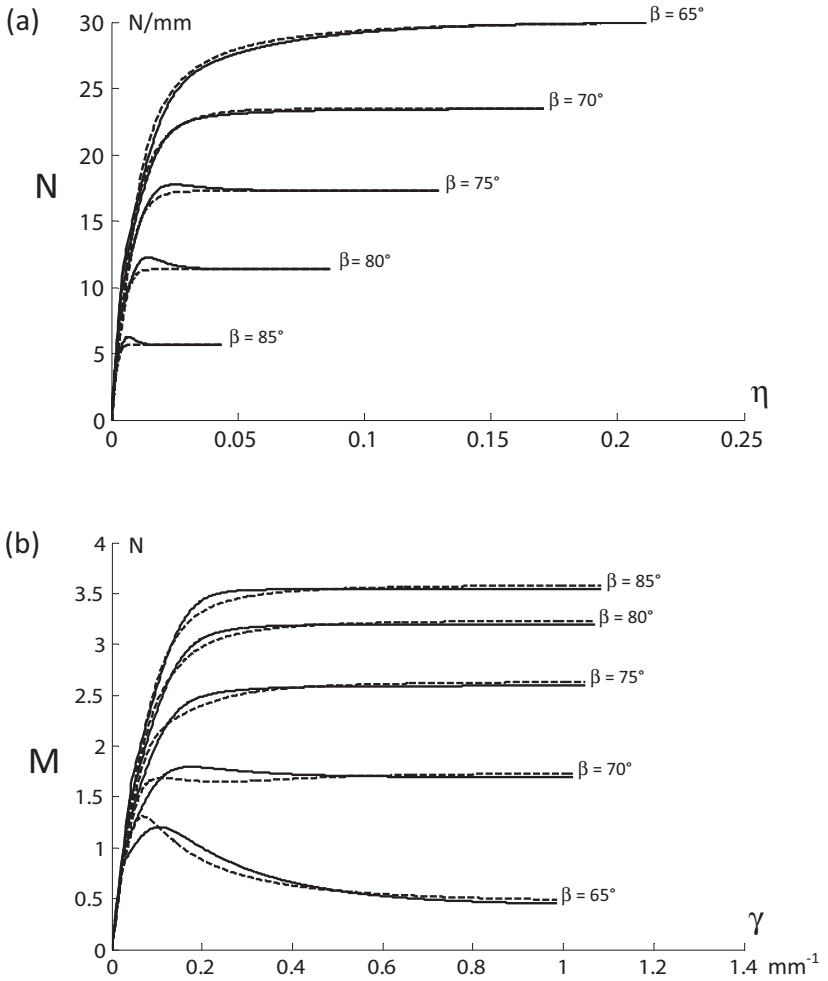

Fig. 10. With reference to the deformation radial paths considered in Figure 9: axial (a) and flexural (b) behaviors of the specimen according to generalized variables model (solid lines) and continuum model (dashed lines).

computed:

$$C_N = E_{11}\,T = 1978\,\mathrm{N/mm},$$
$$C_M = E_{11}\,T^3/12 = 34.88\,\mathrm{N\,mm}$$
$$N_\infty = \sigma_\infty\,T = 32.2\,\mathrm{N/mm},\quad M_\infty = \sigma_\infty\,T^2/4 = 3.70\,\mathrm{N},$$
$$a = T\,N_\infty/M_\infty = 4.$$

It follows that, possibly, only two (i.e., M_0 and κ) among the six parameters of the generalized variables model need to be estimated by the minimization procedure. This simplifies the optimization procedure, but the optimum value of the discrepancy function turns out to be higher. The resulting estimates are: $M_0 = 2.37$ N and $\kappa = 6.00$ and the graphical comparison analogous to that in Figure 9 is visualized in Figure 11. Comparisons between diagrams permit to assess the approximation implied by transition to a generalized variables model for structural analysis of products like boxes, when sandwich test simulations are carried out through FE discretization as solid continua. Clearly, the errors implied depend on the selected constitutive models. The numerical exercises presented in what precedes are merely intended to clarify inverse analysis procedures, not to suggest models for industrial practices.

7. Closing Remarks

In the industrial environments, active on design and production of food containers, tests of foils and laminates involving compression at present turns out to be a nonmarginal research subject.

Some popular constitutive models proposed for paper, e.g., [1], contain parameters that cannot be identified by tension tests, even with cruciform bi-axiality [4]. Models in generalized variables for laminates to be used in boxes also frequently require calibration under compression. The experimental equipment ("sandwich" system) and parameter identification procedure presented in this article might be useful since a variety of tests combining compression and bending on foil specimens could be generated in order to provide input to parameter identification based on computer simulations and on minimization of a discrepancy function with the unknown parameters as variables.

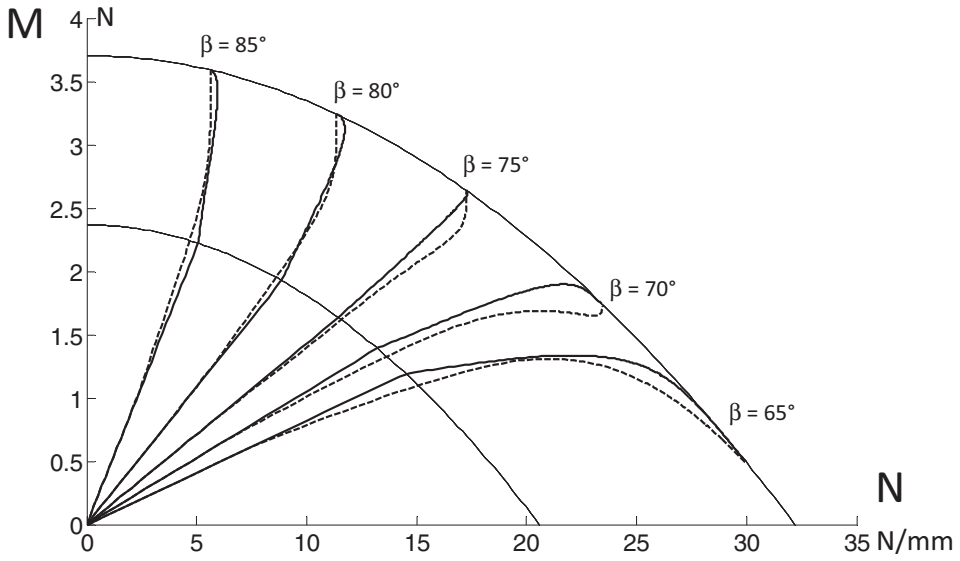

Fig. 11. Behaviors of the specimen cross section orthogonal to MD under imposed generalized strains η and γ along radial paths $\gamma\ T = \eta \tan(\beta)$: according to the generalized variables model calibrated only with respect to yield limit moment M_0 and hardening coefficient κ (solid lines) and according to the earlier calibrated continuum model (dashed lines).

The following main items, proposed in what precedes, are supposed to be novel contributions:

(a) The "sandwich" system preliminarily designed herein by trial-and-error stabilizes and keeps under control the foil specimen under compression.
(b) The consequent interactions between sample and stabilizing blocks are made acceptable by (finite element) simulations of the whole system along the test.
(c) Digital image correlation provides economically a number of sensitive experimental data on system response (many displacements, not only reactions to imposed rotations) so that the parameter identification becomes a well-posed inverse problem.
(d) Computer simulations of the test by the finite element model (b) are performed in order to select by sensitivity analyses the quantities to be measured.
(e) Previous expertise in the industry can usually lead to define, for each category of foils to use, upper and lower bounds on each parameter to estimate (namely, a "search domain" in the space of the sought parameters). Such circumstance, by recourse to the proper orthogonal decomposition procedure, can make fast and economical the parameter estimation.
(f) The foil specimen under sandwich tests is interpreted to practical purposes (like in box design) as beam or plate without homogenization of layers. However, commercial computer codes may prevent finite element models of continua and beams (or shells) interacting in the same structural system. Then, transition from the calibrated material model to parameters of generalized variables model preselected for the foil can be easily performed, as shown in this article, by means of a second simpler parameter identification.

Future developments, now in progress, related to the results presented in this article are mentioned below.

(i) The sandwich shape should be optimized, after the present preliminary design, by means of many test simulations for each foil category of industrial interest.
(ii) Tests of laminate creases, by slightly adjusted sandwich system, will be employed, at least as pseudo-experiments apt to design the procedure, for the identification of the parameters contained in models recently proposed for creases, particularly in [26].
(iii) The possible lack of convexity of the present discrepancy function suggests to investigate also (after first-order optimization algorithm adopted herein with multiple initializations) soft-computing algorithms for routine industrial applications, namely, suitably optimized artificial neural networks (like, e.g., in [4]) or genetic algorithms made fast and economical by the procedure adopted herein (see appendix).
(iv) A stochastic approach (e.g., Kalman filtering) will lead to quantification of the consequences of experimental noise on uncertainties in the resulting estimates (i.e., covariance matrix of the latter resulting from that of the former).

Acknowledgments

Thanks are expressed by the authors particularly to Dr. Roberto Borsari and his co-workers, Dr. Andrea Giampieri and Dr. Alberto Mameli, for fruitful interactions.

Funding

The results presented in this article have been achieved in a research project supported by a contract between Politecnico (Technical University) of Milan and Tetra Pak Company.

References

[1] Q.S. Xia, M.C. Boyce, and D.M. Parks, A constitutive model for the anisotropic elastic–plastic deformation of paper and paperboard, Int. J. Solids Struct., vol. 39, pp. 4053–4071, 2002.

[2] P. Makela and S. Ostlund, Orthotropic elastic–plastic material model for paper materials, Int. J. Solids Struct., vol. 40, pp. 5599–5620, 2003.

[3] J. Castro and M.O. Ostoja-Starzewski, Elasto–plasticity of paper, Int. J. Plast., vol. 19, pp. 2083–2098, 2003.

[4] T. Garbowski, G. Maier, and G. Novati, On calibration of orthotropic elastic-plastic constitutive models for paper foils by biaxial tests and inverse analyses, Struct. Mult. Optim. DOI: 10.1007/s00158-011-0747-3, 2011.

[5] F. Hild and S. Roux, Digital image correlation: from displacement measurement to identification of elastic properties—A review, Strain, vol. 42, pp. 69–80, 2006.

[6] M.A. Sutton, J.J. Orteu, and H.W. Schreier, Image Correlation for Shape, Motion and Deformation Measurements—Basic Concepts, Theory and Applications, Springer, New York, 2009.

[7] J.N. Perie, H. Leclerc, S. Roux, and F. Hild, Digital image correlation and biaxial test on composite material for anisotropic damage law identification, Int. J. Solids Struct., vol. 46, pp. 2388–2396, 2009.

[8] M. Kleiber, H. Antunez, T.D. Hien, and P. Kowalczyk, Parameter Sensitivity in Nonlinear Mechanics: Theory and Finite Element Computations, John Wiley and Sons, New York, 1997.

[9] R.L. Iman and W.J. Conover, Small sample sensitivity analysis techniques for computer models, with an application to risk assessment, Commun. Stat. Theory Meth., vol. 9, pp. 1749–1842, 1980.

[10] L. Luu, Z. Wang, M. Vo, T. Hoang, and J. Ma, Accuracy enhancement of digital image correlation with B-spline interpolation, Optics Lett., vol. 36, pp. 3070–3072, 2011.

[11] A. Chatterjee, An introduction to the proper orthogonal decomposition, Curr. Sci., vol. 78, pp. 808–817, 2000.

[12] Y.C. Liang, H.P. Lee, S.P. Lim, W.Z. Lin, K.H. Lee, and C.G. Wu, Proper orthogonal decomposition and its applications—Part I: Theory, J. Sound Vib., vol. 252, pp. 527–544, 2002.

[13] V. Buljak, Inverse Analysis with Model Reduction—Proper Orthogonal Decomposition in Structural Mechanics, Springer Verlag, Berlin, 2011.

[14] A. Harrysson and M. Ristinmaa, Large strain elasto–plastic model of paper and corrugated board, Int. J. Solids Struct., vol. 45, pp. 3334–3352, 2008.

[15] S. Kaliszky, Plasticity—Theory and Engineering Applications, Elsevier, Amsterdam, 1989.

[16] J. Lubliner, Plasticity Theory, Macmillan, New York, 1990.

[17] M. Ageno, G. Bolzon, and G. Maier, An inverse analysis procedure for the material parameter identification of elastic–plastic freestanding foils, Struct. Mult. Optim., vol. 38, pp. 229–243, 2009.

[18] Abaqus, Reference Manual, version 6.10, 2011.

[19] D. Lecompte, A. Smits, H. Sol, J. Vantomme, and D. Van Hemelrijck, Mixed numerical–experimental technique for orthotropic parameter identification using biaxial tensile tests on cruciform specimens, Int. J. Solids Struct., vol. 44, pp. 1643–1656, 2007.

[20] A.R. Conn, N.I.M. Gould, and P.L. Toint, Trust-Region Methods, Society for Industrial and Applied Mathematics, Philadelphia, 2000.

[21] T.F. Coleman and Y. Li, An interior trust region approach for nonlinear minimization subject to bounds, SIAM J. Opt., vol. 6, pp. 418–445, 1996.

[22] M.D. Buhmann, *Radial Basis Functions*, Cambridge University Press, Cambridge, UK, 2003.

[23] Z. Ostrowski, R.A. Bialecki, and A.J. Kassab, Solving inverse heat conduction problems using trained POD-RBF network, Inv. Prob. Sci. Eng., vol. 16, pp. 705–714, 2008.

[24] Matlab 7.9.0, User Manual. Available from http://www.mathworks.com.

[25] V. Buljak and G. Maier, Proper orthogonal decomposition and radial basis functions in material characterization based on instrumented indentation, Eng. Struct., vol. 33, pp. 492–501, 2011.

[26] A. Giampieri, U. Perego, and R. Borsari, A constitutive model for the mechanical response of the folding of creased paperboard, Int. J. Solids Struct., vol. 48, pp. 2275–2287, 2011.

Appendix: Outline of the Procedure Here Adopted for the Parameter Identification

For the minimization of the discrepancy function $\omega(\mathbf{p})$, Eq. (8), with respect to the parameter vector $\mathbf{p}$, a mathematical programming algorithm has been adopted here, specifically an iterative "first-order" Trust Region Algorithm (TRA) in its version available in MATLAB [25] and described in detail in the literature, see e.g., [20, 21]. The main features of TRA can be outlined as follows: initialization of the iteration sequence concerns a vector (possibly suggested by "experts") within the search domain; each iteration rests on a quadratic programming problem in two variables, namely, along gradient and Newton direction; in each iteration the objective function is a quadratic approximation $\tilde{\omega}$ of the discrepancy function and constraints are provided by a "trust region" and by the original search domain; the quadratic approximation of $\omega(\mathbf{p})$ at the point $\mathbf{p}_k$, reached after k iterative steps, is generated by means of the gradient $\mathbf{g}$, the Jacobian $\mathbf{J}$ of the measurable quantity vector $\mathbf{u}$ as function of the parameter $\mathbf{p}$, and by means of the Hessian matrix $\mathbf{H}$ approximated through the Jacobian, specifically:

$$\begin{aligned}
&\omega(\mathbf{p}_k + \Delta\mathbf{p}_{k+1}) \cong \tilde{\omega}(\Delta\mathbf{p}_{k+1}) = \omega(\mathbf{p}_k) + \mathbf{g}^T \Delta\mathbf{p}_{k+1} \\
&\quad + \frac{1}{2}\Delta\mathbf{p}_{k+1}^T \mathbf{H}\, \Delta\mathbf{p}_{k+1} \\
&\text{where } \mathbf{J} = \frac{d\mathbf{u}}{d\mathbf{p}^T}(\mathbf{p}_k), \quad \mathbf{g} = \frac{d\omega}{d\mathbf{p}}(\mathbf{p}_k) = 2\mathbf{J}^T\mathbf{C}^{-1}[\mathbf{u}(\mathbf{p}_k) - \bar{\mathbf{u}}], \\
&\quad \mathbf{H} \cong 2\mathbf{J}^T\mathbf{C}^{-1}\mathbf{J},
\end{aligned} \tag{A1}$$

where $\Delta\mathbf{p}_{k+1}$ is the variable vector for which the above quadratic programming minimization problem has to be solved as $(k+1)$ step.

The above features of TRA clearly imply first derivatives only, numerically approximated by forward finite differences. Nevertheless, generally a large number of test simulations is required (in each iteration the number of simulations is equal to $P+1$ where P is the number of sought parameters). Therefore, great practical advantages arise from solving each forward problem not by FE simulations but by the POD + RBF method outlined below.

The POD procedure can be briefly outlined as follows (details, e.g., in [12, 13, 23, 25]):

(1) Let the $N \times M$ matrix $\mathbf{U}$ (here with $N \leq M$) gather the above defined "snapshots" $\mathbf{u}_1, \ldots, \mathbf{u}_M$, each one consisting of the values of the N measurable quantities resulting from a FE simulation based on a grid node $\mathbf{p}_i$ ($i = 1,\ldots, M$) over the search domain in the P-dimensional space of the parameters. The N measurable quantities are those which will be measured in the actual test and will be the input

of the inverse analysis leading to the parameter estimates. The M vectors $\mathbf{u}_i$ are supposed to be "correlated" (namely "almost parallel") because of obvious physical reasons rooted in their generation.

(2) The (symmetric and positive-definite or at least positive-semi-definite) matrix $\mathbf{D} = \mathbf{U}^T\mathbf{U}$ of order M (but of rank N, in the case when $N < M$) is generated by the snapshot matrix $\mathbf{U}$. The eigenvalue problem concerning matrix $\mathbf{D}$ is solved, namely its non-zero eigenvalues λ_i and corresponding normalized eigenvectors $\mathbf{v}_i$ are computed and are employed to generate the following ortho-normal matrix, called "basis," of order N, with $\mathbf{I}$ being the identity matrix of order N:

$$\mathbf{\Phi} = [\varphi_1, \ \ldots, \ \varphi_N], \quad \varphi_i = \boldsymbol{U}\, v_i \lambda_i^{-1/2}, \ (i = 1, \ldots, N), \quad \mathbf{\Phi}^T\mathbf{\Phi} = \boldsymbol{I}. \tag{A2}$$

It was analytically demonstrated (see, e.g., [12, 13]) that such $N \times N$ matrix $\mathbf{\Phi}$ represents the "optimal reference" basis in the N-dimensional space of measurable quantities, according to the provision motivated by "snapshots correlation" here pointed out earlier, as expected in a geometrical interpretation of physical circumstances characterizing the present engineering problem. "Optimal reference" means that versor φ_1 maximizes a norm of the projection on it of all snapshots $\mathbf{u}_i$ (in their N-dimensional space); versor φ_2 does the same in the space (of dimensionality $N - 1$) orthogonal to φ_1; and so on in succession.

In the new basis, the snapshots contained in matrix $\mathbf{U}$ can be represented by means of a new $N \times M$ matrix $\mathbf{A}$ of "amplitudes" $\mathbf{a}_i$, namely:

$$\mathbf{u}_i = \mathbf{\Phi}\,\mathbf{a}_i, \ (i = 1, \ldots, M), \quad or \quad \mathbf{U} = \mathbf{\Phi}\mathbf{A}, \quad \text{where } \mathbf{A} = \mathbf{\Phi}^T\,\mathbf{U}. \tag{A3}$$

(3) The above mentioned norms of projections have been demonstrated to be proportional to the eigenvalues λ_i (see, e.g., [12, 13]); therefore, again in view of the snapshots correlation, it is quite natural to neglect in the basis $\mathbf{\Phi}$ the axes corresponding to the smallest eigenvalues, namely, to generate a "truncated" POD basis by preserving $\hat{N} < N$ axes and corresponding amplitudes $\mathbf{a}_i$. Such "truncation" leads to an approximation of the snapshot $\mathbf{u}_i$ ($i = 1, \ldots, M$) governed by the $N \times \hat{N}$ matrix $\hat{\mathbf{\Phi}}$ as "truncated basis" and $\hat{N}$-dimensions vector $\hat{\mathbf{a}}_i$ as "reduced amplitudes":

$$\mathbf{u}_i \simeq \hat{\mathbf{u}}_i = \hat{\mathbf{\Phi}}\,\hat{\mathbf{a}}_i, \ \ (i = 1, \ldots, M), \ \ \text{or} \ \ \mathbf{U} \simeq \hat{\mathbf{U}} = \hat{\mathbf{\Phi}}\,\hat{\mathbf{A}}, \quad \text{where} \ \ \hat{\mathbf{A}} = \hat{\mathbf{\Phi}}^T\,\hat{\mathbf{U}}. \tag{A4}$$

It can be said that matrix $\hat{\mathbf{\Phi}}$ and $\hat{N} \times M$ matrix $\hat{\mathbf{A}}$ contain, as "compressed shape" through optimized approximation, the whole meaningful information on the considered system and on the role in it played by sought parameters: in other terms, the whole cumulative information contained in the results achieved by the set of preliminary computed simulations of the test.

(4) The results achieved in the preceding phase (3) can make fast and economical any test simulation based on any new parameter vector $\mathbf{p}$ included in the preselected search domain. In fact, "Radial Basis Functions" (RBF) g_j formulated for all the nodes in the parameter space $\mathbf{p}_i$, namely, in general form (see, e.g., [22]):

$$g_i\,(\mathbf{p}) \equiv g_i\,(\|\mathbf{p} - \mathbf{p}_i\|), \quad i = 1, \ldots, M, \tag{A5}$$

can be considered as basis functions for the interpolation. The assessment of the approximate snapshot amplitudes $\hat{\mathbf{a}}$ corresponding to a parameter vector $\mathbf{p}$ can now be carried out through RBF interpolation, namely,

$$\mathbf{a}^h\,(\mathbf{p}) = \sum_{j=1}^{M} b_i^h\ g_i\,(\mathbf{p}), \quad h = 1, \ldots, \hat{N}. \tag{A6}$$

The coefficients b_j^h of these linear combinations are computed simply by imposing Eq. (A6) in all parameter nodes $\mathbf{p}_j$, $j = 1,\ldots, M$, and by solving the consequent linear equations, which read in matrix formulation:

$$\hat{\mathbf{A}} = \mathbf{B}\,\mathbf{G}, \quad \text{where} \ \ \mathbf{B} = \left[b_i^h\right], \quad \mathbf{G} = \left[g_j\,\left(\mathbf{p}^h\right)\right]. \tag{A7}$$

(5) When the $M \times \hat{N}$ matrix $\mathbf{B}$ is computed once-and-for-all, for a new parameter set $\mathbf{p}$, the response to the test in terms of measurable quantities, briefly the "snapshot," can be assessed merely by Eqs. (A6) and (A4) in a by-far more economical fashion if compared to FE simulations.